Coupling between Sea Surface Temperature and Low-Level Winds in Mesoscale Numerical Models

QINGTAO SONG AND DUDLEY B. CHELTON

College of Oceanic and Atmospheric Sciences, and Cooperative Institute for Oceanographic Satellite Studies, Oregon State University, Corvallis, Oregon

STEVEN K. ESBENSEN, NICOLAI THUM, AND LARRY W. O'NEILL

College of Oceanic and Atmospheric Sciences, Oregon State University, Corvallis, Oregon

(Manuscript received 19 February 2008, in final form 3 July 2008)

ABSTRACT

This study evaluates the impacts of sea surface temperature (SST) specification and grid resolution on numerical simulations of air–sea coupling near oceanic fronts through analyses of surface winds from the European Centre for Medium-Range Weather Forecasts (ECMWF) model. The 9 May 2001 change of the boundary condition from the Reynolds SST analyses to the NOAA Real-Time Global (RTG) SST in the ECMWF model resulted in an abrupt increase in mesoscale variance of the model surface winds over the ocean. In contrast, the 21 November 2000 change of the grid resolution resulted in an abrupt increase in mesoscale variability of surface winds over mountainous regions on land but had no significant effect on winds over the ocean.

To further investigate model sensitivity to the SST boundary condition and grid resolution, a series of simulations were made with the Weather Research and Forecasting (WRF) model over a domain encompassing the Agulhas return current (ARC: also called "retroflection") region in the south Indian Ocean. Results from three WRF simulations with SST measured by the Advanced Microwave Scanning Radiometer on the Earth Observing System *Aqua* satellite (AMSR-E) and the Reynolds and RTG SST analyses indicate the vital importance of the resolution of the SST boundary condition for accurate simulation of the air–sea coupling between SST and surface wind speed. WRF simulations with grid spacings of 40 and 25 km show that the latter increased energy only on scales shorter than 250 km. In contrast, improved resolution of SST significantly increased the mesoscale variability for scales up to 1000 km.

Further sensitivity studies with the WRF model conclude that the weak coupling of surface wind speeds from the ECMWF model to SST is likely attributable primarily to the weak response of vertical turbulent mixing to SST-induced stability in the parameterization of boundary layer turbulence, with an overestimation of vertical diffusion by about 60% on average in stable conditions and an underestimation by about 40% in unstable conditions.

1. Introduction

The western boundary current systems (e.g., the Gulf Stream, the Kuroshio, the Agulhas Current) and their eastward extensions into the interior oceans play an important climatic role by transporting warm subtropical water poleward with a large transfer of heat from the ocean to the atmosphere. The associated large temperature gradients at the edges of the currents, owing to their enormous source of heat and moisture, produce significant changes of wind speed, temperature and turbulent fluxes in the marine atmospheric boundary layer (MABL) from one side of a sea surface temperature (SST) front to the other, with an increase (decrease) in wind speed as the wind blows from cold (warm) to warm (cold) water across the front (e.g., Sweet et al. 1981; Businger and Shaw 1984; Friehe et al. 1991; Giordani et al. 1998; Lee-Thorp et al. 1999; Chelton et al. 2001, 2004; Park and Cornillon 2002; O'Neill et al. 2003, 2005; Park et al. 2006; Song et al. 2006). Satellite observations have revealed that this ocean–atmosphere interaction occurs throughout the World Ocean wherever SST fronts exist. The objective of this study is to investigate the ability of numerical models to simulate the observed SST influence on surface winds.

Corresponding author address: Qingtao Song, College of Oceanic and Atmospheric Sciences, Oregon State University, 104 COAS Admin. Bldg., Corvallis, OR 97331-5503.
E-mail: qsong@coas.oregonstate.edu

DOI: 10.1175/2008JCLI2488.1

As reviewed by Xie (2004), Chelton et al. (2004), and Small et al. (2008), a strong influence of SST on surface winds is consistently observed on scales shorter than about 1000 km from Quick Scatterometer (QuikSCAT) observations of surface winds and Advanced Microwave Scanning Radiometer (AMSR) observations of SST in regions of strong SST gradients associated with ocean currents. It has been found from a number of studies using these satellite observations (Chelton et al. 2001; O'Neill et al. 2003, 2005; Chelton 2005; Chelton and Wentz 2005; Maloney and Chelton 2006) that 1) the wind speed perturbations are linearly related to SST perturbations, 2) horizontal wind divergence is linearly related to the downwind SST gradient, and 3) wind curl is linearly related to the crosswind SST gradient. Depending on the resolution of the SST fields used as the bottom boundary condition, most research mesoscale models and operational numerical weather prediction (NWP) models successfully reproduce a positive correlation between surface wind speed anomalies and SST anomalies (Small et al. 2003; Song et al. 2004; Chelton et al. 2004; Small et al. 2005; Chelton 2005; Chelton and Wentz 2005; Haack et al. 2005; Maloney and Chelton 2006; Spall 2007; Haack et al. 2008; O'Neill et al. 2008, manuscript submitted to *J. Climate*). These studies have generally found that the strength of this coupling is underestimated in numerical models.

Of particular interest to this study, the coupling between SST and low-level wind is clearly represented in the surface wind fields from the European Centre for Medium-Range Weather Forecasts (ECMWF) model when averaged over time periods long enough to remove the effects of energetic weather variability (e.g., over a few weeks or longer). The SST boundary condition in the ECMWF model was changed on 9 May 2001 from the Reynolds SST fields to higher-resolution National Oceanic and Atmospheric Administration (NOAA) Real-Time Global (RTG) SST fields. Chelton (2005), Chelton and Wentz (2005), and Maloney and Chelton (2006) conducted analyses of the surface wind speed variability before and after the SST change in the ECMWF model with reference to the National Centers for Environmental Prediction (NCEP) surface wind analyses. They found that the spatial resolution and accuracy of the ECMWF surface wind fields significantly improved immediately after this change in the SST boundary condition. However, the response of the ECMWF wind stress to SST perturbations is only about half as large as is observed in the satellite data, which the authors speculated is due, at least in part, to inadequacies in the parameterization of boundary layer processes.

Similar conclusions have been reached by Brown et al. (2005, 2006) who compared the wind turning across the MABL in the ECMWF model and the Met Office model with that in radiosonde and QuikSCAT observations. They found that the ECMWF model underestimates surface wind response to SST and that the sensitivity of vertical mixing to static stability is underestimated in the ECMWF planetary boundary layer (PBL) parameterization.

It has been suggested that model grid resolution is as important as the resolution of SST in the surface boundary condition to the accuracy and resolution of surface winds over the ocean (P. Janssen 2007, personal communication). On 21 November 2000, the ECMWF model spectral resolution was improved from T319 to T511, corresponding to a grid resolution improvement from about 60 km to about 40 km. It is well established that higher resolution can produce more realistic modeling of small-scale features, for example, a better representation of orography and coastal regions, and more accurate synoptic and subsynoptic dynamics such as frontal properties and tropical cyclones and hurricanes. The importance of grid resolution in the vicinity of strong SST fronts has not yet been investigated.

The purposes of this study are 1) to clarify the effects of SST resolution and model grid resolution on the surface wind fields in mesoscale numerical models, 2) to directly assess the impact of the SST boundary condition on air–sea coupling on scales shorter than 1000 km, and 3) to explore the possible reasons for the underestimation of the SST influence on surface winds in the ECMWF global forecast model through a series of sensitivity experiments made with the Weather Research and Forecasting (WRF) model. To isolate the SST influence that is of interest here, the model simulations are averaged over a month.

2. The resolution of sea surface temperature fields

Previous studies have demonstrated the importance of a realistic SST boundary condition for properly simulating wind variability on scales shorter than about 1000 km. The SST products (Reynolds SST analyses, NOAA Real-Time Global SST analyses, and AMSR SST observations) used as the surface boundary condition in the numerical simulations for this study are briefly summarized in this section. More detailed descriptions of these SST fields can be found in Chelton (2005) and Chelton and Wentz (2005, and references therein).

The widely used Reynolds SST analyses are based on a blending of in situ observations from buoys and ships and satellite observations from the infrared Advanced Very High Resolution Radiometer (AVHRR). The analyses are constructed by optimum interpolation

(OI) that uses correlation length scales of approximately 900 km zonally and 600 km meridionally. This low spatial variation was adopted in order to avoid sampling errors because of the sparse distribution of in situ observations and data loss from cloud contamination in the satellite infrared observations. Based on the same in situ and satellite data as those used in Reynolds OI analyses, the NOAA NCEP Real-Time Global SST uses smaller geographically varying and isotropic correlations length scales ranging from 100 km for regions of strong SST gradients to 450 km for regions of weak SST gradients. The improvement in spatial resolution of RTG SST analyses over Reynolds SST analyses is remarkable in regions of strong SST gradients such as the Agulhas return current (ARC) region that is the focus in this study (Chelton and Wentz 2005, Figs. 2 and 6). However, because of unavoidable biases and sampling errors in the AVHRR data associated with the persistent cloud coverage and very sparse in situ SST data, the accuracies of satellite infrared-based SST fields are questionable in the ARC region. The AMSR measures horizontally and vertically polarized brightness temperature at six microwave frequencies across a single 1445 km swath. AMSR SST is estimated in near all-weather condition with an ~50 km footprint size (see Chelton and Wentz 2005 for details). SST measurements from microwave satellite radiometers overcome the sampling biases and errors of infrared measurements because of the transparency of clouds to microwave radiation. The effective spatial resolution is thus substantially improved.[1]

Examples of SST fields in the ARC region averaged over the month of July 2002 are shown in Fig. 1. The SST fields were spatially high-pass filtered by applying a loess filter with half-power filter cutoff wavelengths of 10° latitude by 30° longitude to remove large-scale SST fields. The abilities of the three SST datasets to resolve the mesoscale features associated with ARC meanders are clearly distinguishable in their power spectral density (Fig. 1d). Scales shorter than about 1000 km are very poorly resolved by Reynolds SST analyses. The spatial resolution of RTG SST is greatly improved in the mesoscale range between 1000 and 250 km. However, the details of small-scale (shorter than 250 km) features are poorly represented by RTG SST compared with the higher-resolution AMSR SST fields.

[1] The OI parameters of the Reynolds infrared-based SST analyses have recently been dramatically reduced, resulting in SST fields with spatial resolution somewhat better than that of the RTG SST fields but not as good as that of microwave-based SST fields (Reynolds et al. 2007). These new Reynolds SST fields are now available from 1985 to the present.

3. Analysis of the ECMWF surface winds

Examination of the small-scale variability in the ECMWF 10-m wind speed fields in the Kuroshio Extension, Agulhas return current, the Gulf Stream, and South Atlantic (not shown here) for December of 1999 and 2000 (before and after the November 2000 change of ECMWF model grid resolution) indicates no visual evidence of any significant differences over the open ocean between these two time periods. However, Chelton and Wentz (2005) and Maloney and Chelton (2006) documented significant increases in small-scale variability before and after the May 2001 change of SST boundary condition from Reynolds to RTG SST in the ECMWF model in the Gulf Stream and ARC region.

The much greater importance of the SST boundary condition to the resolution of 10-m wind fields over the ocean is easily seen from the continuous record of 4-times-daily ECMWF surface wind fields from July 1999 to July 2006, a time period that bridges the dates of both of the major model changes. Time series of the small-scale spatial variance of 10-m wind speed from overlapping 2-month averages at 1-month intervals for the ARC region show about an order of magnitude increase in small-scale variance after the May 2001 change of the SST boundary condition (Fig. 2). However, the November 2000 grid resolution change had no detectable effect on the small-scale variability of 10-m winds over the ocean. The time series in the Kuroshio Extension region (Fig. 3) also indicate a significant increase in small-scale variability of 10-m winds over the ocean after the change of the SST boundary condition, but no detectable difference after the change of the model grid resolution.

The effects of the two major changes of the ECMWF model considered herein on the small-scale variability of low-level winds in the ECMWF model are further clarified in Fig. 4 from the time series of the spatial variance of surface wind speed fields on scales shorter than about 1000 km over all continental landmasses and over the open ocean (Kuroshio Extension, Agulhas return current, the Gulf Stream, and South Atlantic). It is apparent that the change of the SST boundary condition resulted in a significant increase in small-scale variability over the open ocean but not over land. In contrast, the change in model grid resolution resulted in a significant increase in small-scale variability of the surface wind field over land, but not over the ocean. The increase in small-scale variability of the wind field over land is particularly strong in mountainous regions (not shown) because they are better represented by the increased grid resolution.

The time series of the small-scale variance of SST

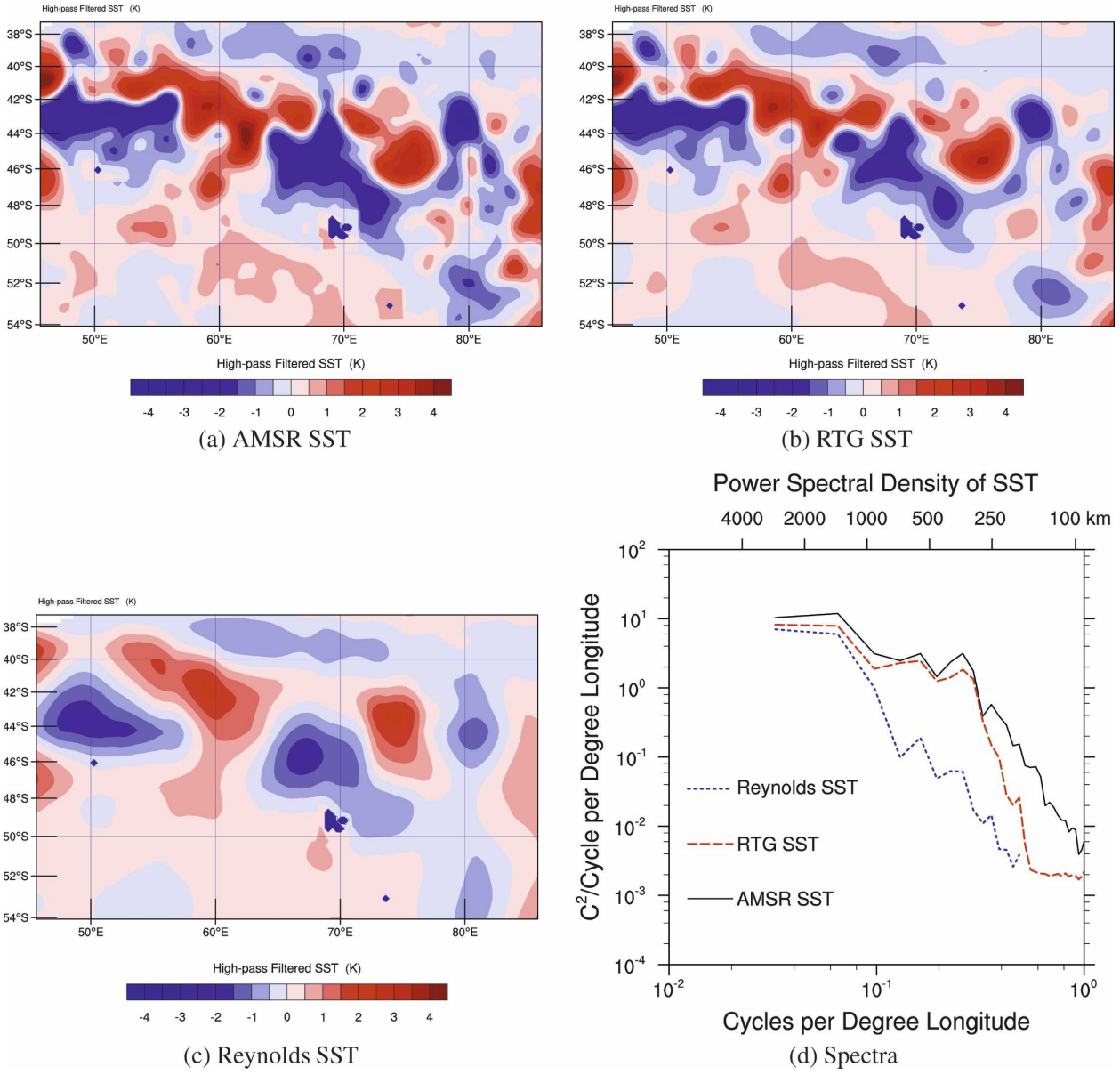

FIG. 1. (a)–(c) Maps of mesoscale SST fields in the Agulhas return current region averaged over July 2002. The SST fields were spatially high-pass filtered to remove wavelength scales larger than 10° latitude by 30° longitude. (d) Zonal wavenumber power spectral density of the spatially high-pass filtered SST fields computed over the region 47°–38°S, 46°–85°E.

from Reynolds analyses, RTG analyses and AMSR observations in the bottom panel of Fig. 4 shows that the RTG variance is about twice that of Reynolds and nearly as large as the AMSR variance. The more accurate representation of small-scale SST variability in the RTG analyses used after 9 May 2001 as the surface boundary condition in the ECMWF model evidently had a dramatic effect on small-scale variability in the ECMWF surface wind fields over the ocean. This sensitivity of surface winds to the resolution of the SST boundary condition is investigated in more detail from the mesoscale model simulations in section 5a.

4. WRF model configuration and experiment design

The sensitivity of mesoscale variance to the SST boundary condition and grid resolution can be investigated in detail using the Weather Research and Forecasting modeling system version 2 (Skamarock et al.

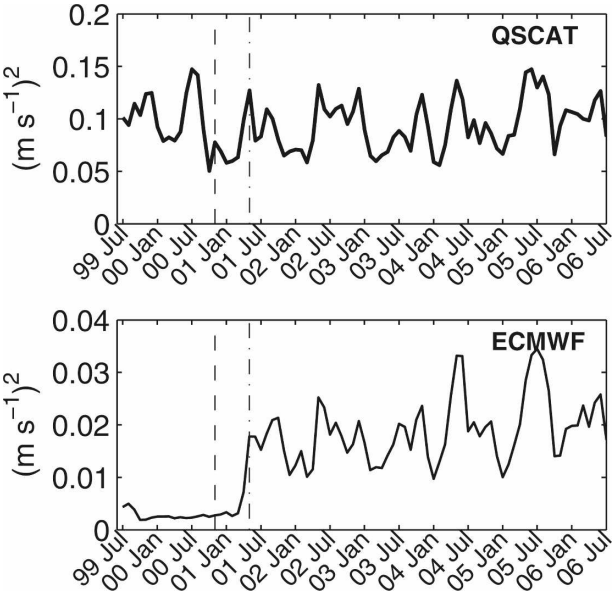

FIG. 2. Time series of the spatial variance of surface wind speed over wavelengths shorter than 1000 km from overlapping 2-month averages at 1-month intervals for the ARC region from (top) QuikSCAT and (bottom) ECMWF. The dashed line corresponds to the 21 Nov 2000 date when the ECMWF grid resolution was improved from T319 to T511, while the dash–dotted line refers to the 9 May 2001 change from Reynolds to RTG SST as the ocean boundary condition in the ECMWF model. Note the different scales of the ordinates of the two panels; the small-scale variability in the QuikSCAT observations is about a factor of 5 stronger than in the ECMWF model after May 2001 and about 50 times stronger prior to that.

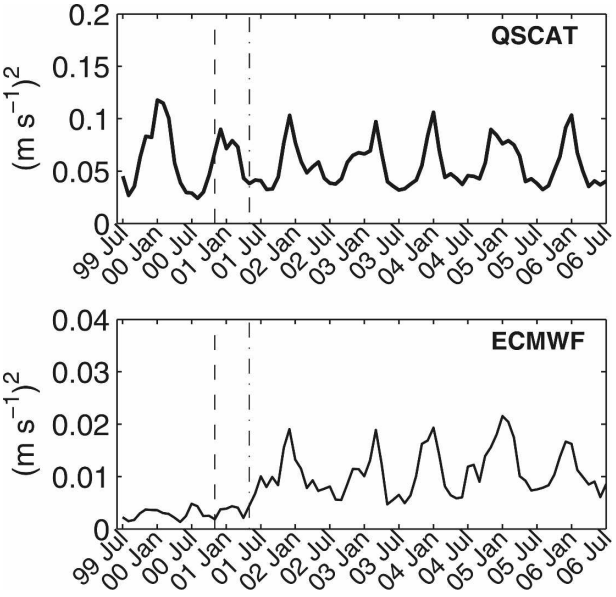

FIG. 3. As in Fig. 2 but for the Kuroshio Extension region.

2005) with the Advanced Research WRF (ARW) dynamic solver, which is the dynamic core available to the WRF model that integrates the compressible, nonhydrostatic Euler equations on a terrain-following mass vertical coordinate. Physical options for all of the model experiments include the simple WRF single-moment 3-class (WSM3) scheme that resolves the water vapor, ice, and precipitation processes, and the modified version of the Kain–Fritsch scheme to represent subgrid-scale effects of convection and shallow clouds. Nonhydrostatic dynamics with a three-dimensional (3D) Coriolis force were used.

It is widely recognized that the PBL plays a critical role in mesoscale weather variability. WRF contains three different PBL schemes to represent the boundary layer processes. The model was run using each PBL scheme, and the surface wind speed was compared with the QuikSCAT observations. The results obtained using the PBL scheme developed by Grenier and Bretherton (2001, hereafter GB01; see also Bretherton et al. 2004) best approximated the QuikSCAT winds. The GB01 PBL scheme was therefore selected for the following experiments, with modification as described below in section 6b to investigate the sensitivity of SST influence on surface winds to the stability dependence of vertical mixing. The GB01 PBL scheme offers several advantages over other boundary layer schemes. It attempts to simulate the tight coupling between cloud formation, convective turbulence, and radiative and surface fluxes. It can handle the internal stratification of a cloud-topped boundary layer (Grenier and Bretherton 2001), meaning that it is able to resolve several convective layers within the MABL.

The WRF model has recently been used to investigate the momentum balance for surface winds (L. W. O'Neill et al. 2008, unpublished manuscript) in the open ocean region southeast of the republic of South Africa. The conclusions of these studies are that SST influences both wind speed and direction through its effects on vertical turbulent mixing and the surface pressure field. The reader is referred to these studies for the details.

For the analyses presented herein, the WRF model was configured with two nested domains. The outer domain encompasses the ARC region that separates the cold Southern Ocean from the warmer Indian Ocean. The inner model domain extends meridionally from 54° to 37°S and zonally from 46° to 86°E, encompassing part of the ARC. A total of 50 vertical levels were used for both outer and inner domains, with finer vertical grid spacing in the boundary layer. The model was also run with 69 vertical levels. The results showed insignificant changes from the 50-level model runs.

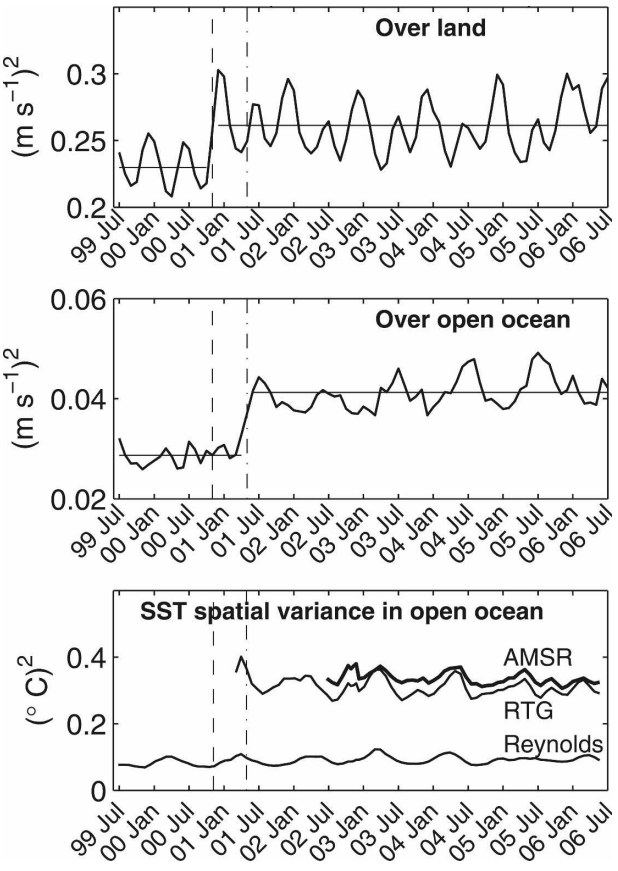

FIG. 4. Time series of the spatial variance of surface wind speed fields on scales shorter than about 1000 km over (top) land and (middle) the open ocean regions. (bottom) Time series of the spatial variance of SST fields on scales shorter than about 1000 km from three sources: Reynolds, RTG, and AMSR. The dashed line corresponds to 21 Nov 2000 when the ECMWF grid resolution was improved from T319 to T511, while the dash–dotted line refers to the 9 May 2001 change from Reynolds to RTG SST as the ocean boundary condition in the ECMWF model. The small-scale variability was isolated by spatial high-pass filtering the wind speed fields with half-power filter cutoffs of 10° longitude by 10° latitude.

Therefore, only model simulations with 50 vertical levels are presented in this manuscript.

The initial fields and boundary condition around the perimeter of the outer nested domain of the WRF model for the 30-day WRF model simulation were obtained from NCEP Global Data Assimilation System (GDAS). The global final analyses consist of simulations over the entire globe on a 1.0° × 1.0° grid of the spectral medium-range forecast model. Spectral modes are interpolated on pressure levels and are available every 6 h.

The experiments conducted to investigate the effects of grid resolution and specification of the SST boundary condition on air–sea coupling on scales shorter than 1000 km are summarized in Table 1. High spatial resolution AMSR SST data were used to force the WRF model to examine the surface wind response to SST in the ARC region in July 2002. The analyses are compared to those from simulations made with RTG SST and Reynolds SST analyses. To examine the sensitivity of the mesoscale air–sea coupling, three model experiments forced by Reynolds SST were conducted with grid spacing of 40 km, 25 km, and 15 km. The SST field was kept constant throughout each model integration. All of the experiments used identical physical process schemes; the only differences between the model runs were either the SST boundary condition or the grid spacing.

TABLE 1. The numerical experiments for investigation of the model sensitivity to grid resolution and SST specification.

Grid spacing (km)	Reynolds SST	RTG SST	AMSR SST
15	√		
25	√	√	√
40	√		

The period of July 2002 was selected based on the fact that the observed annual cycle of air–sea coupling is strongest in the ARC region during austral winter (Fig. 2, see also O'Neill et al. 2005). The analyzed results from the 30-day WRF experiments were averaged over the last 28 days to allow a spinup time of 2 days at the beginning of each simulation. Unless specified otherwise, July 2002 refers to the period 3–31 July 2002.

5. Model results

a. Sensitivity to SST specification

The performance of the WRF model with a grid spacing of 25 km is validated with the surface winds observed by QuikSCAT (Fig. 5). Scatterometers respond to wind stress at the sea surface as opposed to wind speed, hence the primary product derived from QuikSCAT data, and used in this study, is the neutral equivalent wind 10 m above the sea surface; that is, the wind speed at 10 m that would produce the observed surface stress if the atmosphere were neutrally stable. The differences between neutral equivalent wind speed and 10-m wind speed are less than 0.5 m s^{-1} in the ARC region for this study (the average bias between these wind speeds is 0.057 m s^{-1}); however, they can be large for atmospheric stratifications that deviate greatly from neutral. The neutral equivalent winds from the WRF simulation were thus used in Figs. 5 and 6 to facilitate the comparison with QuikSCAT surface winds.

The spatially high-pass filtered AMSR SST fields are

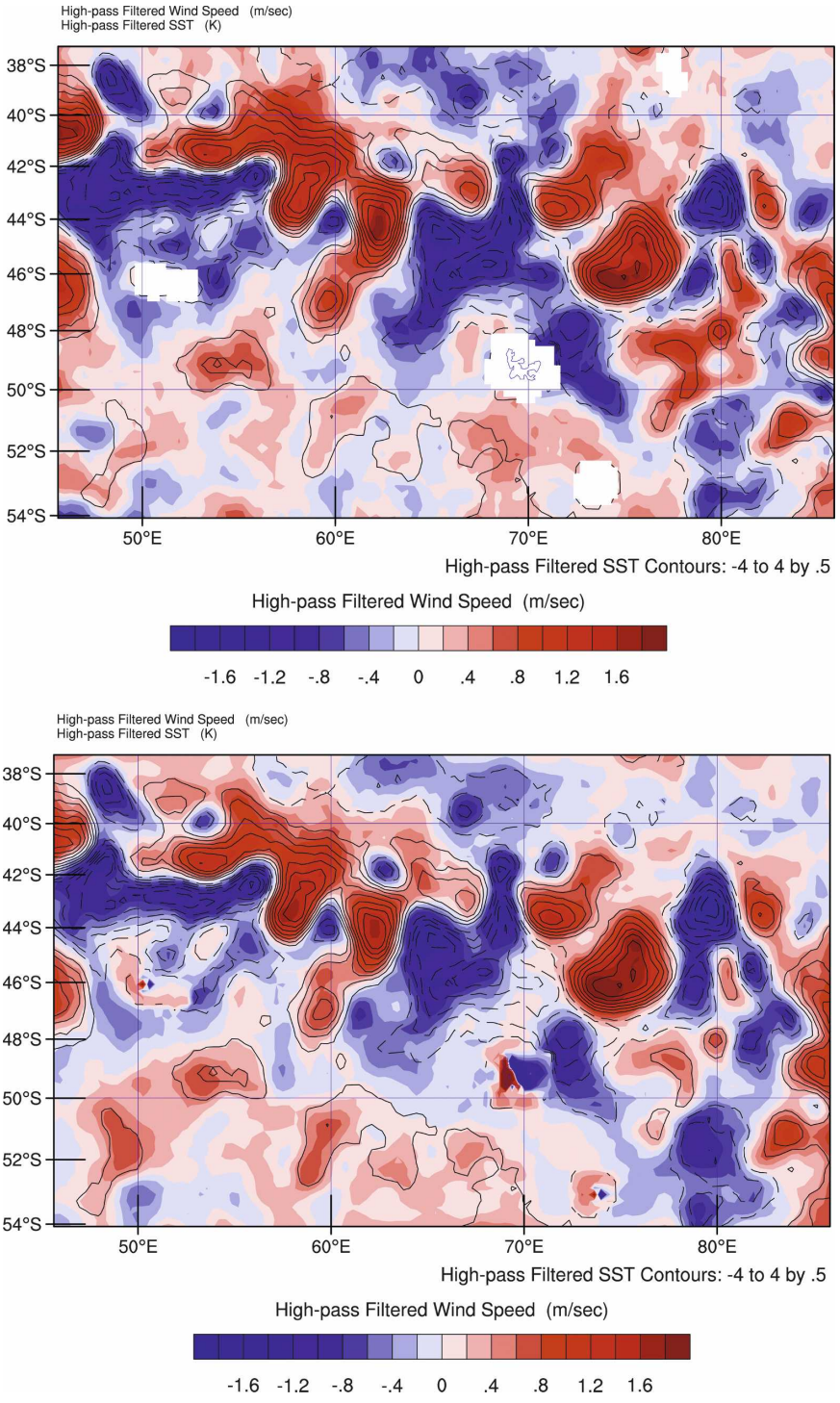

FIG. 5. Maps of spatially high-pass filtered neutral equivalent wind speed 10 m above the sea surface (color) from (top) QuikSCAT and (bottom) WRF simulation and AMSR SST (contours, with a contour interval of 0.5°C) in the ARC region averaged over July 2002. The stability response factor $R_s = 1.0$ was used for the WRF simulation (see section 6b).

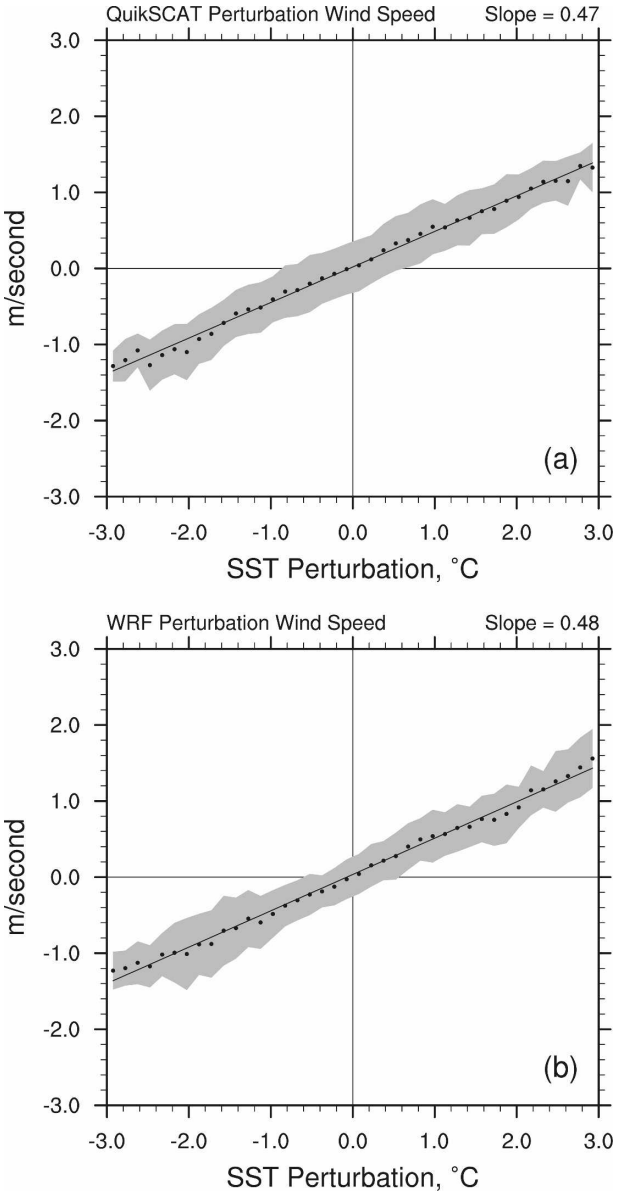

FIG. 6. Binned scatterplots of the relationships between the perturbation 10-m neutral equivalent wind speed and perturbation AMSR SST computed over the region 47°–38°S, 46°–85°E: (top) QuikSCAT observations and (bottom) WRF results. The points are the means within each bin over July 2002, and the shaded zones are ±std dev of the means within each bin. The lines through the points represent least square fits of the binned means. The stability response factor R_s = 1.0 was used for the WRF simulation.

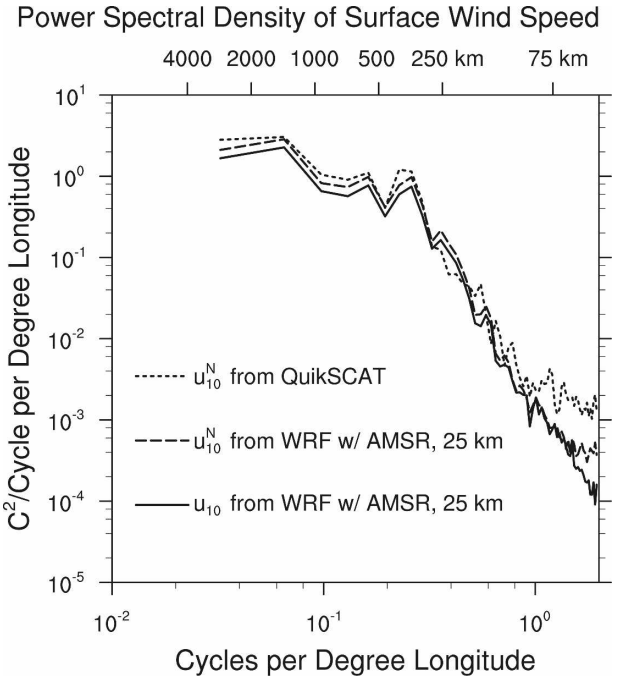

FIG. 7. Zonal wavenumber power spectral density of spatially high-pass filtered 10-m wind speed (u_{10}) and neutral equivalent 10-m wind speed (u_{10}^N) from the 25-km WRF simulation and QuikSCAT u_{10}^N computed over the region 47°–38°S, 46°–85°E. The stability response factor R_s = 1.0 was used for the WRF simulation (see section 6b).

overlaid as contours on the spatially high-pass filtered surface wind speeds in the ARC region. Both the model results and the QuikSCAT observations show a tight coupling between the SST and surface winds. The effects of SST-induced changes of surface wind speeds are statistically quantified in the binned scatterplot of neutral equivalent wind perturbations (u_{10}^N) as a function of SST perturbations shown in Fig. 6. Results from both the WRF simulation with the AMSR boundary condition and the QuikSCAT observations indicate a linear response of surface wind speed to SST with very similar coupling coefficients (slope of the straight-line least square fit) computed from the binned scatterplots. The coupling coefficient calculated from the WRF simulation of 10-m wind speed (u_{10}) was 0.42, compared to the value of 0.48 in Fig. 6 calculated for u_{10}^N. The reason that u_{10}^N results in a larger coupling coefficient is that u_{10}^N is somewhat larger than u_{10} for the slightly unstable atmospheric stratification usually found over the ocean (Tang and Liu 1996). The differences between u_{10} and u_{10}^N from WRF model simulation and u_{10}^N from QuikSCAT are further quantified by the zonal wavenumber power spectral densities in Fig. 7. On scales from about 250 to 2000 km, WRF u_{10}^N is in closer agreement with QuikSCAT than is WRF u_{10}. It is thus important to use neutral equivalent winds to make a direct comparison with scatterometer winds. Note that the flattening of the power spectral density of WRF u_{10}^N at the highest wavenumbers is likely round off errors associated with the u_{10}^N offline calculation. The flattening of QuikSCAT winds on scales shorter than about

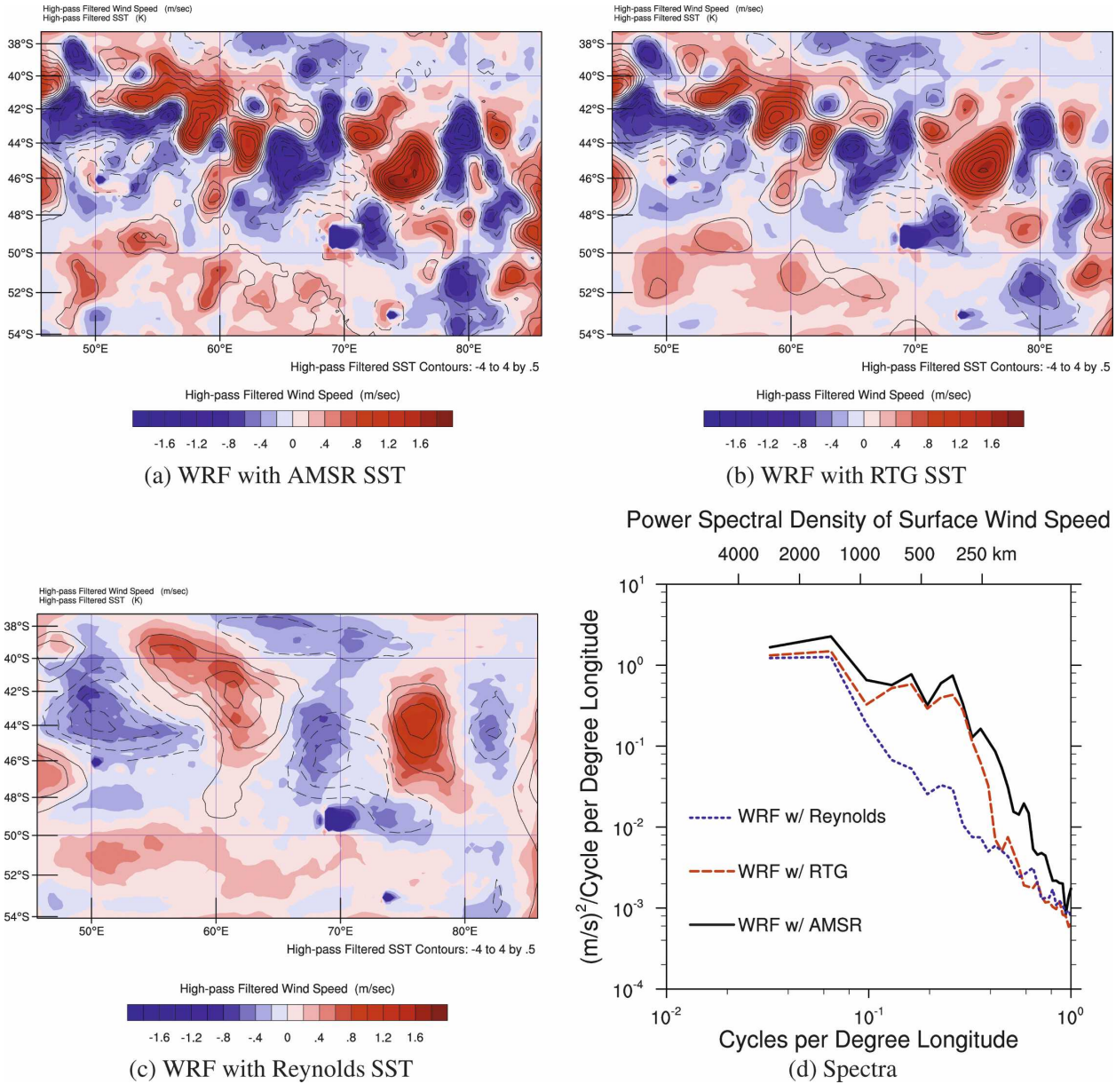

FIG. 8. (a)–(c) Maps of spatially high-pass-filtered 10-m wind speed (color) from three WRF simulations and their corresponding SST fields (contours, with a contour interval of 0.5°C) in the ARC region averaged over July 2002. (d) Zonal wavenumber power spectral density of the spatially high-pass-filtered 10-m wind speed computed over the region 47°–38°S, 46°–85°E. The stability response factor $R_s = 1.0$ was used for the WRF simulations.

100 km is primarily due to the QuikSCAT measurement noise. In the subsequent comparison of WRF winds with QuikSCAT winds, the focus is on the scales larger than 100 km over which QuikSCAT measurement noise is insignificant.

The spatially high-pass filtered surface wind speed field obtained from the WRF simulation with RTG SST as the surface boundary condition (Fig. 8b) is generally similar to the results from the simulation forced by high-resolution AMSR SST (Fig. 8a) except that it is somewhat smoother; the latter adds more small-scale details of the structure of the air–sea interaction. This is quantified by the power spectral densities of surface wind speed in Fig. 8d. The surface wind forced with the RTG SST boundary condition is a factor of 2–8 times less energetic on scales shorter than about 250 km compared with the AMSR-forced surface wind.

The simulated wind speed field using Reynolds SST

as the bottom boundary condition (Fig. 8c) shows very weak coupling on scales shorter than 1000 km compared to those obtained with either AMSR SST or RTG SST (Figs. 8a and 8b). Although it generally retains the large-scale features of air–sea coupling, the mesoscale variability in the surface wind field is completely lost. This is because the Reynolds SST fields themselves have very little variability on scales shorter than about 1000 km (Fig. 1d).

The comparisons of the three simulations in Fig. 8 indicate that the resolution of the SST fields is a key component in the accuracy of air–sea coupling in the model simulations. For scales larger than 1000 km, surface wind speed spectra from all three simulations are similar in magnitude. For scales shorter than 1000 km, most of the energy in the 28-day average considered here results from the SST forcing, with simulated spectral characteristics that are very similar to those of SST fields (cf. Figs. 8d and 1d). Mesoscale kinetic energy in surface wind fields is thus dominated by SST forcing on the time scales of the 28-day average considered here. The lack of sub-1000-km-scale features in the Reynolds SST fields results in severely deficient kinetic energy in the surface wind field on these scales. RTG SST greatly improves the representation of the mesoscale features in the wind field associated with the ARC, but it lacks variability on scales shorter than about 250 km. Consequently, the kinetic energy of surface wind speed is underestimated on scales shorter than about 250 km in the WRF model simulation forced by RTG SST.

b. Sensitivity to grid resolution

Three WRF experiments were performed using Reynolds SST with grid spacings of 40 km, 25 km, and 15 km to investigate the sensitivity of the model to grid resolution. We adopted the definition of effective resolution of a model from Skamarock (2004) as the wavelength at which the spectrum of a model wind field begins to decay relative to the observed spectrum or relative to the spectrum from a higher-resolution model simulation that resolves high-wavenumber variability before numerical dissipation leads to decay. This "feature resolution" of numerical models is usually a factor of 5 or more coarser than the grid spacing of the model (Pielke 1991; Grasso 2000; Walters 2000; Durran 2000). For the WRF simulation with the Reynolds SST boundary condition, it is evident from Fig. 9 that the 40-km grid spacing has an effective resolution of about 250 km, when compared with the simulations with 25 and 15 km grid spacing. This is a factor of 6 times larger than the grid spacing. It is also evident from Fig. 9 that, compared with the simulation with a 15-km grid, the effective resolution of the WRF simulation with Reynolds SST boundary condition and 25-km grid spacing has an effective resolution of about 100 km, that is, about a factor of 4 larger than the grid spacing.

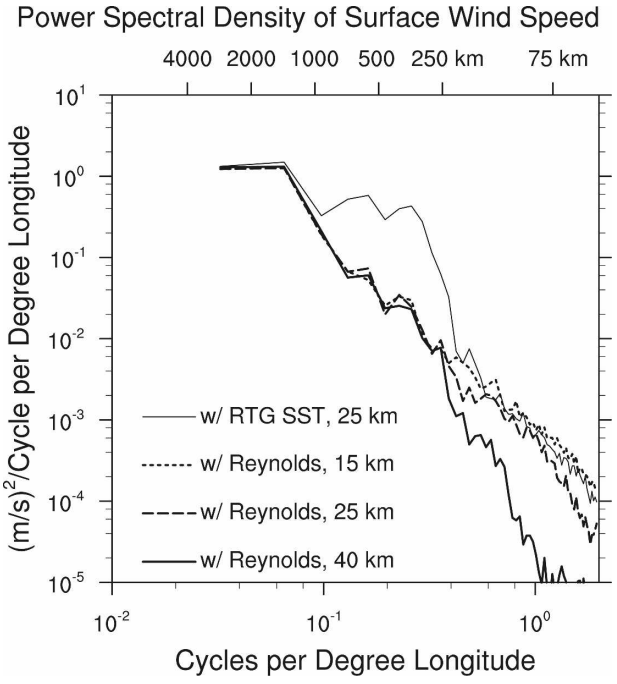

FIG. 9. Zonal wavenumber spectra of 10-m wind speed from four WRF sensitivity experiments with different SST fields and different grid resolutions computed over the region 47°–38°S, 46°–85°E in the ARC for July 2002. The stability response factor R_s = 1.0 was used for the WRF simulations.

It is evident from Fig. 8d and from the thin solid line in Fig. 9 that the resolution of the SST field is far more important than the grid resolution for simulation of air–sea coupling in the mesoscale between 250 and 1000 km. For the air–sea coupling that is the focus of this study, an appropriate SST field that realistically represents the mesoscale features of ocean currents is thus vitally important. The choice of 25-km grid resolution is sufficient to resolve these features in the AMSR SST fields and to simulate the response of the surface mean wind field. A higher grid resolution does not improve the model representation of the mesoscale air–sea coupling when forced by RTG SST fields.

6. Comparisons with ECMWF simulated surface wind

The surface wind fields constructed from the 6-hourly wind fields from the operational ECMWF model were averaged over July 2002, the same period as the WRF simulations considered in sections 4 and 5, and were then spatially high-pass filtered with the same

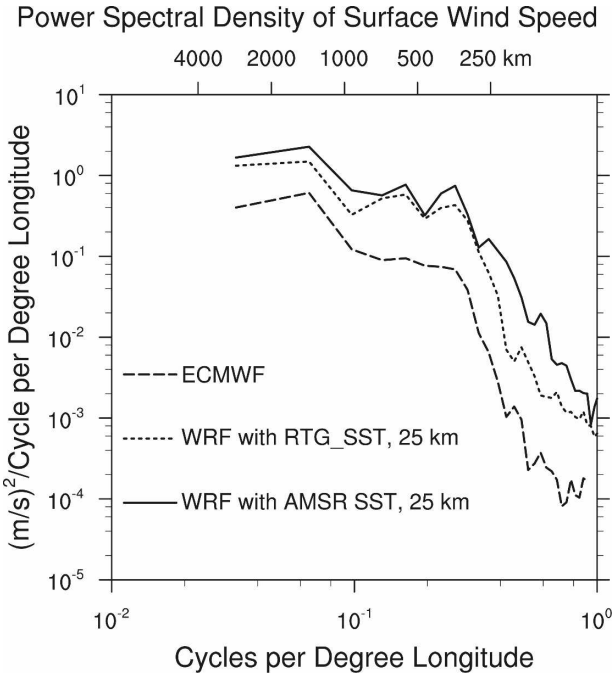

FIG. 10. Zonal wavenumber spectra of 10-m wind speed from ECMWF (long dashed line), WRF with AMSR SST at 25-km grid spacing (solid line), and WRF with RTG SST at 25-km spacing (short dashed line). The 10-m wind speed spectra were computed over the region 47°–38°S, 46°–85°E in the ARC for July 2002. The stability response factor $R_s = 1.0$ was used for the WRF simulations.

30° longitude and 10° latitude filter cutoff wavelengths applied above to the WRF simulations. All of the model-produced surface wind fields exhibit positive spatial correlation between wind speed perturbations and SST perturbations. The zonal wavenumber power spectral density of the ECMWF high-pass filtered surface wind speeds is compared with those computed from the WRF simulated surface winds forced with the AMSR SST and RTG SST in Fig. 10. As described in section 5, the WRF simulation with AMSR SST as surface boundary condition produced the best approximation to the QuikSCAT observation. For the period considered for this study, the ECMWF model used the RTG SST analyses. It is evident from Fig. 10 that the WRF simulation with the RTG SST boundary condition contains considerably more energetic variability on all spatial scales relative to the ECMWF model.

There are a number of possible reasons for the lower variance of ECMWF surface wind speed in the wavenumber spectra. Although experience at ECMWF suggests that the accuracy of medium-range forecasts has steadily improved with increasing resolution, the ECMWF forecast model is known to implement a relatively strong horizontal diffusion that damps high wavenumber energy. Cavaleri et al. (1997) found a steady underestimation of the ECMWF wind speeds in the Adriatic Sea by about 30% that they attributed to the strong horizontal diffusion in the ECMWF model. By comparing the latent heat fluxes obtained in situ from various cruises, Rouault et al. (2003) reported that latent heat fluxes from the ECMWF model were significantly underestimated by about 20% in the vicinity of the ARC region. The underestimation of heat fluxes could be due to deficiencies of the air–sea flux algorithm and/or turbulent heat exchange in the MABL. Brown et al. (2005) found that the ECMWF PBL parameterization had excessive vertical mixing in stable conditions that resulted in systematic errors in surface wind direction over the sea. Brown et al. (2006) identified systematic errors in the ECMWF wind directions in conditions of warm advection with unstable boundary layers. Horizontal diffusion, vertical mixing, grid resolution, and inadequacies in the resolution of the SST boundary condition are therefore all candidate explanations for the low mesoscale variance of the 28-day average ECMWF surface winds.

To isolate the contributors that could account for the underestimation of variance in the ECMWF surface wind speeds compared to QuikSCAT observations, we performed a series of exploratory sensitivity experiments using the WRF model with different grid spacing, different horizontal diffusion, and different vertical diffusion. We then determined which combination gave results closest to the ECMWF model. The 25-km WRF simulation with RTG SST as the surface boundary condition and the GB01 parameterization of vertical mixing considered in section 5 was selected as the baseline simulation since RTG SST was used as the boundary condition in the ECMWF model during the July 2002 time period considered here. It is evident from Fig. 10 that the surface wind speeds from the WRF baseline simulation are in much better agreement with QuikSCAT observations than with the ECMWF model. This baseline simulation used the sixth-order filter for horizontal diffusion recommended within the WRF modeling system (Skamarock et al. 2005).

a. Sensitivity to horizontal diffusion in the WRF model

Horizontal diffusion in mesoscale models serves to control small-scale noise and to avoid numerical instabilities. High-wavenumber noise can arise either from computational errors associated with discretization of the governing equations that describe the evolution of the state of the atmosphere, or from dynamical inconsistencies when the models are initiated with real data

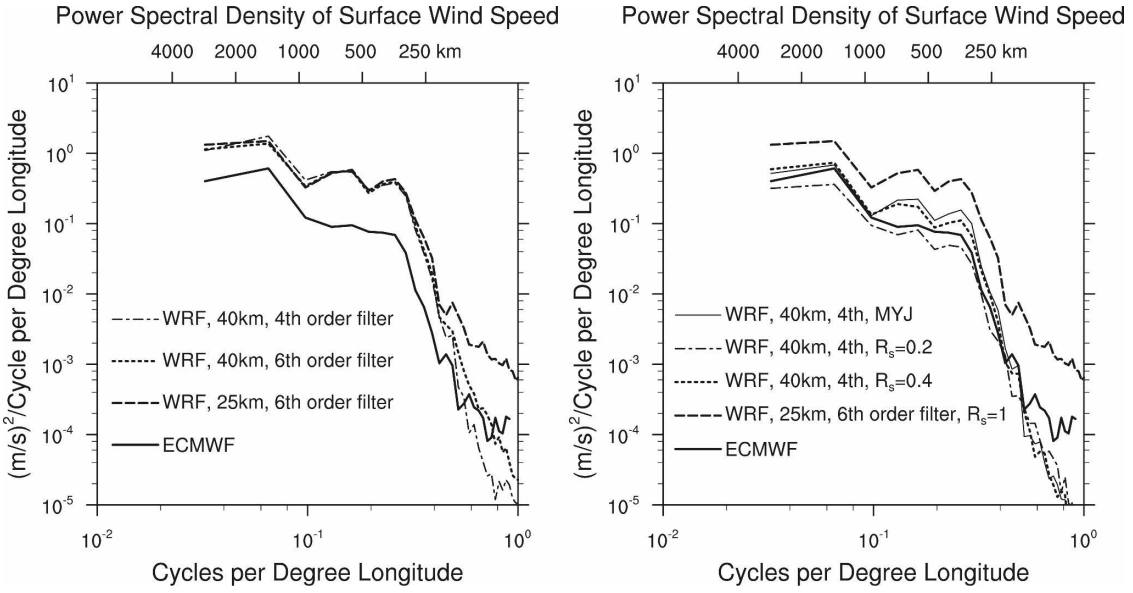

FIG. 11. Zonal wavenumber spectra of surface wind speed from ECMWF and WRF experiments: (left) with $R_s = 1.0$ and various grids and horizontal diffusion filters and (right) with different stability response factors R_s defined in Eq. (3) and different boundary layer schemes. RTG SST fields were used for all the simulations as surface boundary condition. The spectra were computed over the same region and period as in Fig. 10.

or from parameterized physical processes. The removal of kinetic energy at high wavenumbers is necessary to avoid buildup of noise variance and unphysical behavior at very small scales. However, it is undesirable to overdamp small-scale features that are physically realistic. This is especially a concern for examining the small-scale features of air–sea coupling that are of interest here.

The WRF model utilizes an implicit horizontal diffusion in its integration and advection schemes in addition to explicit horizontal diffusion. The third-order Runge–Kutta (RK3) time integration scheme selected in the WRF experiments for this study can be used stably with high-order approximations to the flux-form advection scheme. If an odd-ordered advection approximation is used, the RK3 scheme has a built-in horizontal filter of the next highest order. For example, if using a fifth-order advection approximation, a sixth-order filter is used to remove high-wavenumber energy.

The ECMWF forecast model uses a spectral dynamic core in which the horizontal distribution of the atmospheric variables is described with a series of spherical harmonics. For the period July 2002, the ECMWF operational model used the T511 version with a triangular truncation of 511 waves in the horizontal, corresponding to a grid spacing of about 39 km. A linear horizontal diffusion of fourth order was used in the ECMWF model.

For consistency with the ECMWF model grid spacing and RTG SST boundary condition of the ECMWF model, the WRF model was forced by RTG SST with a 40-km grid spacing. To approximate the horizontal diffusion used in the ECMWF model, a WRF experiment was performed with the horizontal diffusion option changed from the baseline sixth-order filter to a fourth-order filter.

The zonal wavenumber power spectral densities of the spatially high-pass filtered surface wind speeds from the ECMWF model and the three WRF experiments are shown in the left panel of Fig. 11. As in the results presented in section 5, changing the grid spacing of the baseline experiment with sixth-order diffusion from 25 to 40 km substantially damps kinetic energy for scales shorter than about 250 km. The change of horizontal diffusion from sixth to fourth order further damps the kinetic energy at the higher wavenumber portion of the spectra because the sixth-order diffusion is less dissipative. The sixth-order diffusion only dissipates at the highest wavenumbers, thus increasing the effective resolution of the model.

These sensitivity experiments indicate that the 40-km grid and increased horizontal diffusion result in significantly reduced kinetic energy on small scales. However, neither of these changes in the WRF model has any significant effect on the wind field on scales longer than about 250 km. While grid resolution and horizontal diffusion may account for some of the underestimation of variance in the ECMWF model on scales smaller than

250 km, they cannot account for the general underestimation of variance on all scales in the ECMWF model. This suggests that the underestimation of surface wind speed variance in the ECMWF model is likely attributable primarily to inadequacies in the parameterization of boundary layer mixing. This is investigated below.

b. Sensitivity to vertical diffusion in the WRF model

In their studies on the air–sea coupling over the ARC region, O'Neill et al. (2005) and Maloney and Chelton (2006) reported that the coupling coefficient between ECMWF wind stress anomalies and SST anomalies is only half as large as the satellite observations. Positive (negative) SST anomalies have a tendency to destabilize (stabilize) the airflow in the MABL and subsequently to alter the vertical turbulent mixing. This suggests that the response of vertical mixing to SST-induced stability may be underestimated in the ECMWF boundary layer scheme. Our methodology here is to change the vertical diffusion in the GB01 PBL scheme by modifying its response to the SST-induced stability, and then compare the resulting surface wind speeds with those from the ECMWF model.

The GB01 PBL scheme is a 1.5-order turbulent closure model in which the turbulent fluxes of temperature, moisture, and momentum within the PBL are computed using an eddy diffusion coefficient K_h for the conserved thermodynamic variables and an eddy diffusivity K_m for the horizontal velocity components. Following Mellor and Yamada (1982, hereafter MY82), K_h and K_m are related to the turbulent kinetic energy (TKE) e, a master turbulent scale l, and a stability function S_h or S_m as

$$K_{h,m} = S_{h,m} l \sqrt{e}. \tag{1}$$

In the GB01 scheme, the vertical transport of TKE is greatly enhanced in order to obtain proper matching of the TKE profile with large eddy simulations (LES) of various convective PBLs. The turbulent length scale is formulated separately for the convective PBL and the situation where the PBL is stably decoupled. Vertical diffusion in the GB01 scheme has a strong dependence on stability compared with the original MY82 PBL scheme.

In this subsection, new parameters, which we refer to as the reduced stability functions Q_h and Q_m, are introduced to represent the efficiency of the response of eddy turbulent diffusion to static stability. Analogous to Eq. (1), the eddy diffusivity is related to Q_h and Q_m and the stability functions $S_h^N$and S_m^N for neutral static stability by

$$K_{h,m} = Q_{h,m} l \sqrt{e}, \tag{2}$$

$$Q_{h,m} = S_{h,m}^N + R_s(S_{h,m} - S_{h,m}^N). \tag{3}$$

The stability function $S_{h,m}$, formulated identical to Eqs. (24)–(26) of Galperin et al. (1988), are functions of the stability parameter G_H defined as

$$G_H = -\left(\frac{l}{e}\right)^2 \beta g \frac{\partial \theta}{\partial z}, \tag{4}$$

where g is the gravitational acceleration, β is a constant equal to 1/273, and θ is potential temperature. For neutrally stable conditions, G_H is set to 0 and the values of S_h^N and S_h^N are 0.49 and 0.39, respectively. The stability response factor R_s in Eq. (3) modulates the vertical diffusion of heat and momentum by an extent that depends on how much the static stability deviates from neutral conditions. When R_s is set to 1, $K_{h,m}$ are equivalent to those in GB01 scheme. A large value of R_s indicates that vertical mixing is more strongly dependent on stability. Values of $R_s < 1$ decrease the dependence of vertical mixing on stability.

Based on the results of the simulations of the effects of the changes of grid resolution and horizontal diffusion considered in section 6a, a 40-km grid spacing and fourth-order horizontal diffusion were used in WRF experiments with various values of stability response factor R_s. The same upper limits for $K_{h,m}$ as in the original GB01 PBL scheme were used to avoid the instabilities associated with the strong mixing when R_s is larger than 1. The values of the stability response factor R_s in Eq. (3) that yielded the WRF simulation that best matched the ECMWF wind field were inferred from the power spectra of ECMWF surface wind speeds (left panel of Fig. 11).

The power spectral densities of spatially high-pass filtered wind speeds from the baseline simulation (WRF with RTG SST, 6th-order horizontal filter, and 25-km grid spacing), WRF simulations with 4th-order filtering, 40-km grid spacing and R_s of 0.4 and 0.2, and the ECMWF model are shown in the right panel of Fig. 11. The surface wind spectrum computed from the WRF simulation with the Mellor–Yamada–Janjic (MYJ) PBL scheme (MY82; Janjic 2002; thin solid line in Fig. 11) has weaker vertical mixing than the GB01 scheme, corresponding approximately to that of the WRF GB01 simulation with a reduced stability response factor of $R_s = 0.4$. The variance of surface wind speeds decreases with decreasing R_s. It is apparent from Fig. 11 that a stability response factor between 0.2 and

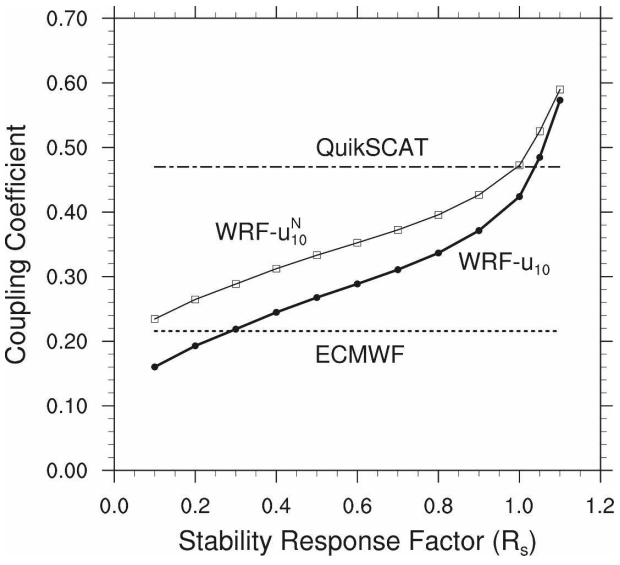

FIG. 12. Dependence of the coupling coefficients of perturbation WRF surface wind speed and perturbation RTG SST on stability response factor R_s. The coupling coefficient is computed from the least square fit of binned means as shown in Fig. 6. Thick solid line is for WRF surface wind speed (u_{10}) and thin solid line is for WRF neutral equivalent wind 10 m above the sea surface (u_{10}^N).

0.4 would produce the best agreement of surface wind speeds in the WRF and ECMWF models.

The coupling coefficients between WRF perturbation wind speeds (10-m wind u_{10} and neutral equivalent wind u_{10}^N) and perturbation SST are plotted in Fig. 12 as a function of stability response factor R_s with reference to those computed from QuikSCAT and the ECMWF model (see Fig. 6 for the QuikSCAT estimate). Consistent with O'Neill et al. (2005) and Maloney and Chelton (2006), the coupling coefficient from the ECMWF model is only half as large as is observed by the QuikSCAT scatterometer winds and AMSR SST. As described in section 5a, the coupling coefficient between perturbation u_{10}^N and perturbation SST is larger than that computed from u_{10}. For $R_s = 1.0$, the WRF coupling coefficient is 0.48 from u_{10}^N. Given that the WRF model does a reasonable job in simulating the QuikSCAT winds, it can be inferred that the coupling coefficient would be about 0.42 if 10-m wind speed could be obtained from QuikSCAT, that is, 12% less than that computed from u_{10}^N. Consistent with reduced variability of surface wind speed, the coupling between wind speed and SST steadily decreases when the response of vertical mixing to the SST-induced stability is weakened in the WRF experiments. In agreement with the spectra in Fig. 11, the WRF experiment with $R_s = 0.3$ produced a coupling coefficient between u_{10} and SST that is nearly identical to that obtained from the ECMWF 10-m surface wind speed. The 28-day average wind speed field in the WRF experiments with R_s equal to 0.3 is shown along with 28-day average ECMWF surface wind speed field in Fig. 13.

While quantitative assessment of the underestimation/overestimation of the eddy diffusivity in the ECMWF model cannot be made in this study, Figs. 11 and 12 suggest that vertical mixing in the ECMWF model is similar to that obtained from with the WRF model using Eqs. (2) and (3) and a value of $R_s = 0.3$. The reduced stability functions, Q_h and Q_m, for heat and momentum are plotted as functions of the stability parameter G_H in Fig. 14 for the original GB01 scheme (when $R_s = 1.0$) and the modified GB01 scheme with reduced stability response factor 0.3. The sensitivity of vertical mixing to stability is substantially reduced for $R_s = 0.3$. From weighted averaging over the values of G_H in the 28-day average WRF simulation for stable conditions, Q_m and Q_h increase by about 60% relative to the original stability function. In conditions in which the PBL is unstable, Q_h and Q_m both decrease by a weighted average of 40%.

The WRF simulations and the thick line in Fig. 14 thus suggest that the ECMWF T511 model underestimates vertical mixing in the boundary layer in the unstable conditions that are usually found over the oceans, resulting in underestimates of surface wind speed. The vertical mixing in less common conditions of stable stratification is overestimated, resulting in overestimates of surface wind speed.

7. Conclusions

We have presented an analysis of the sensitivity of simulated air–sea coupling between mesoscale surface winds and small-scale SST variability to the resolution of the SST boundary condition, grid resolution, horizontal diffusion, and vertical diffusion. Analyses of the ECMWF surface winds distinguish the effects of SST resolution and grid resolution on the mesoscale variability of surface wind fields over the ocean in the ECMWF model. Time series of the spatial variance of the ECMWF surface wind speed fields on scales shorter than about 1000 km show that the 9 May 2001 change of the ocean surface boundary condition from coarse-resolution Reynolds to high-resolution RTG SST analyses in the ECMWF model resulted in an abrupt increase in small-scale variance of surface winds over the ocean. In contrast, the 21 November 2000 change of the grid resolution had no significant effect on winds over the ocean, although it resulted in an abrupt increase in the small-scale variance of surface winds over continents, especially near mountains.

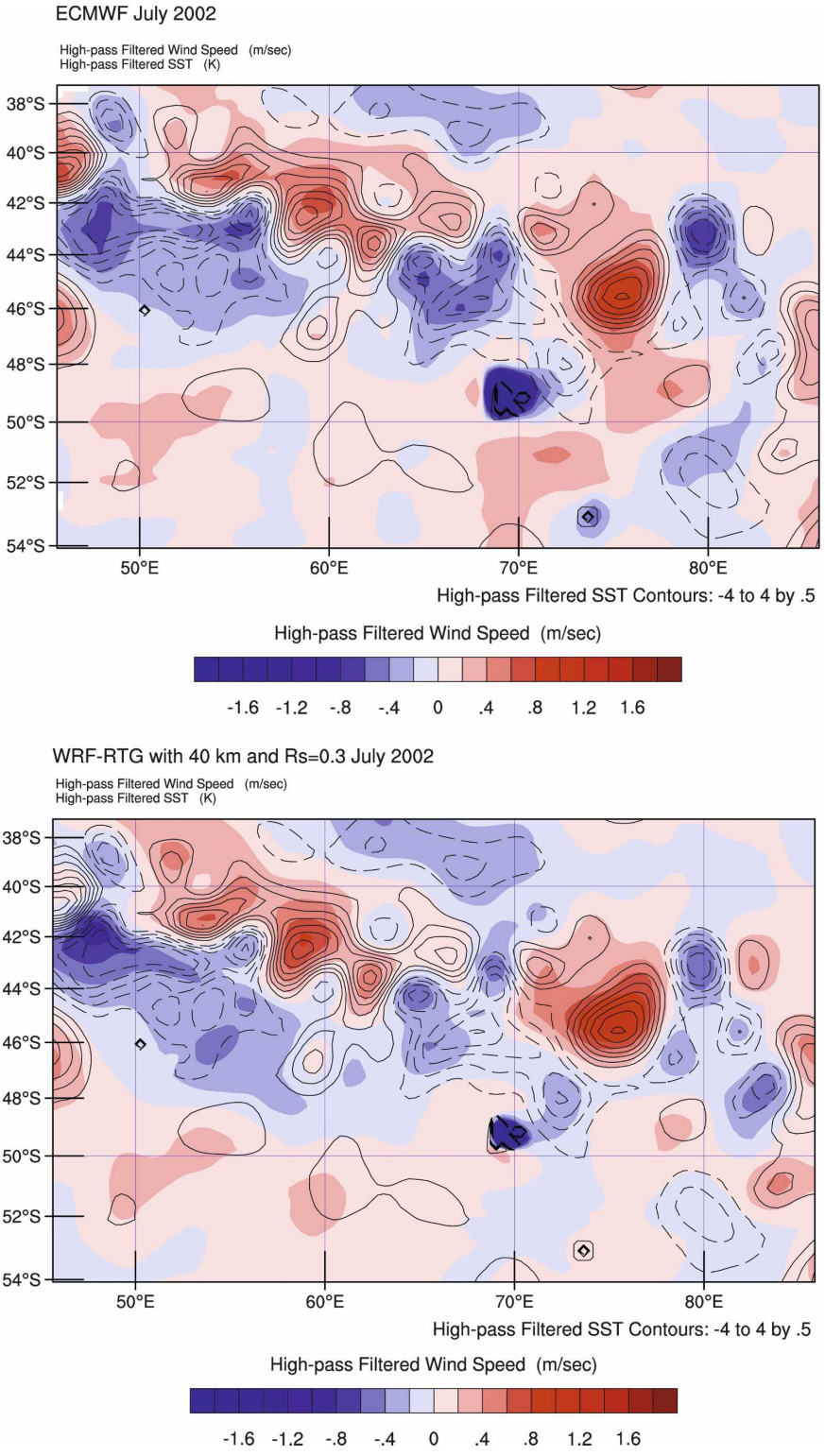

FIG. 13. Maps of spatially high-pass-filtered wind speed (color) from (top) ECMWF and (bottom) WRF RTG simulation when stability response factor is set to $R_s = 0.3$. Contours are spatially high-pass-filtered RTG SST fields with a contour interval of 0.5°C in the ARC region averaged over July 2002.

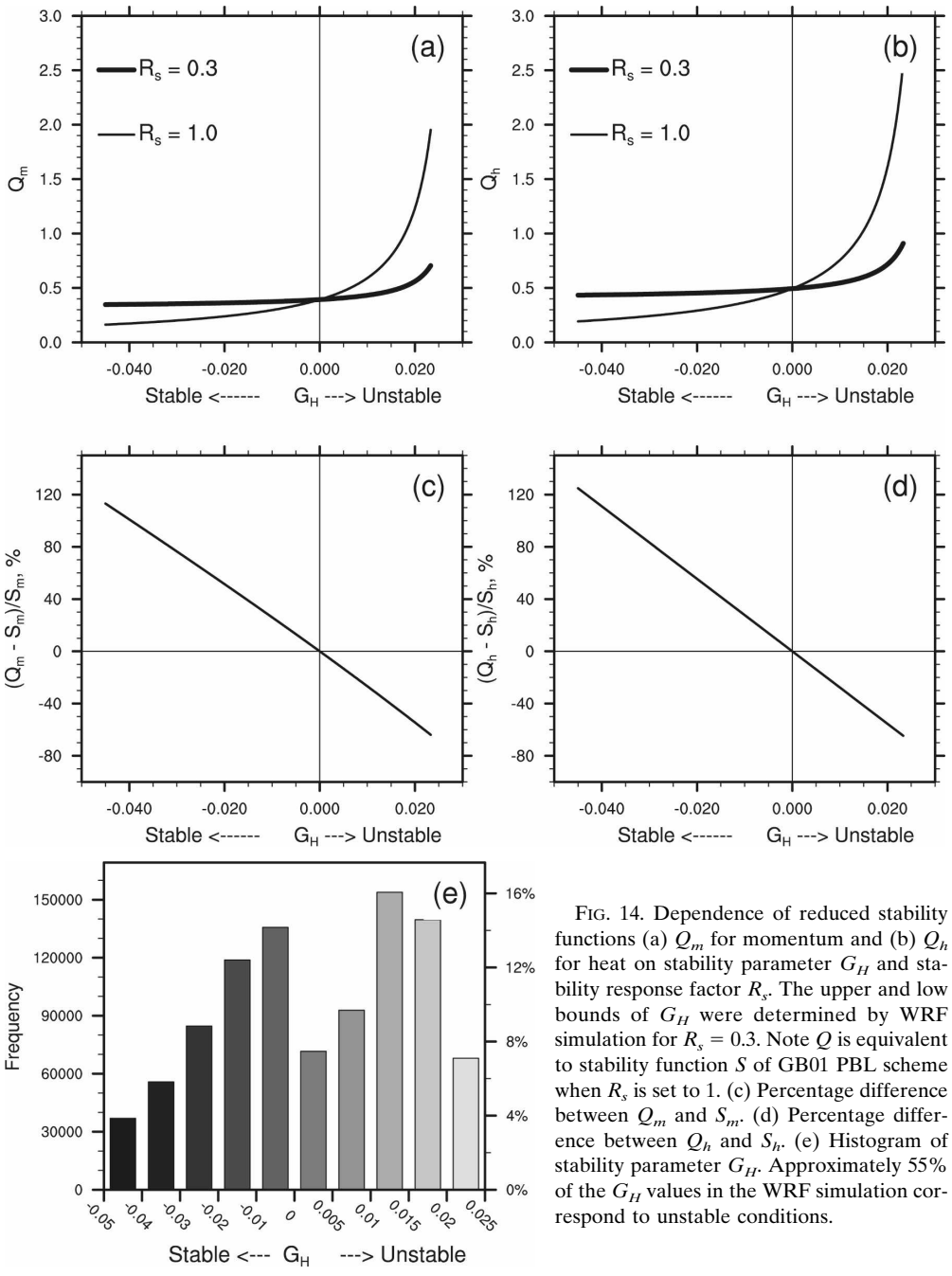

FIG. 14. Dependence of reduced stability functions (a) Q_m for momentum and (b) Q_h for heat on stability parameter G_H and stability response factor R_s. The upper and low bounds of G_H were determined by WRF simulation for $R_s = 0.3$. Note Q is equivalent to stability function S of GB01 PBL scheme when R_s is set to 1. (c) Percentage difference between Q_m and S_m. (d) Percentage difference between Q_h and S_h. (e) Histogram of stability parameter G_H. Approximately 55% of the G_H values in the WRF simulation correspond to unstable conditions.

The impact of the SST boundary condition and model grid resolution on coupling between SST perturbations and surface wind speed perturbations was further investigated from a series of sensitivity experiments performed with the mesoscale WRF model. The WRF numerical experiments in section 5 are consistent with the time series of small-scale variance of the ECMWF wind speeds. Our analyses of ECMWF wind fields and WRF experiments indicate that mesoscale air–sea coupling is sensitive to the resolution of the SST boundary condition. If the grid spacing is chosen to allow full representation of the SST features, mesoscale air–sea coupling is insensitive to increased grid resolution. It is thus necessary to run models with a high-resolution SST boundary condition to faithfully simulate the air–sea coupling observed in satellite data.

SST gradients and mountains have similar impacts on

the sub-1000-km kinetic energy. They both increase the surface forcing to the atmosphere, causing horizontal distribution of the airflow above the surface. Just as the influence of topography on low-level winds is strong in regions of strong topographic gradients, the coupling between surface winds and SST is strong in regions of strong SST gradients associated with ocean currents. Improved grid resolution accompanied by a better representation of the surface forcing (orography over land or SST gradients over the ocean) can result in small-scale energy increase in the low-level wind fields.

While the small-scale variability of surface winds in the ECMWF model increased after the 9 May 2001 change to the higher-resolution RTG SST boundary condition, it was only about half as large as in the QuikSCAT observations. The reasons for the low variance of the ECMWF T511 surface wind speeds were explored in this study through comparisons of the ECMWF surface wind speeds with those from a series of WRF studies conducted in section 6. Our results indicate that the grid resolution change from 25 to 40 km damps kinetic energy, but the influence is mostly restricted to scales shorter than the effective resolution of $\sim 6\Delta x$ for mesoscale models ($\sim$250 km for a grid spacing of $\Delta x = 40$ km). The fourth-order horizontal diffusion further damps energy for scales shorter than about 250 km. On the other hand, a small reduction in the dependence of vertical mixing on SST-induced stability results in significantly reduced kinetic energy on all scales in the WRF simulations considered in this study. This suggests that the vertical diffusion coefficients parameterized in the ECMWF PBL scheme are underestimated for the unstable conditions usually found over the ocean and overestimated for stable conditions.

To improve the accuracy of model representations of mesoscale air–sea coupling in regions of strong SST gradients associated with major western boundary currents and their extensions into the interior ocean, the resolution and accuracy of the SST boundary forcing and the accuracy of model parameterizations of vertical mixing in the marine atmospheric boundary layer (MABL) response to SST are leading-order factors. With increasing grid resolution and the resulting weaker horizontal diffusion, the accuracy of small-scale air–sea coupling can be further improved because less energy is damped on small scales. However, the improvement is restricted to scales shorter than about six times the model grid spacing.

Our findings of the underestimation (overestimation) of vertical mixing in the boundary layer in unstable (stable) conditions in the ECMWF operational model are consistent with the conclusions of Brown et al. (2005, 2006), who found that the response of the surface winds to changing stability is underestimated in the ECMWF model. Recent upgrades to the boundary layer scheme in the Met Office operational global NWP model with a reduction in the vertical mixing in stable conditions and an increase in the vertical mixing in unstable conditions resulted in significant improvements in the dependence of low-level winds on changing stability (Brown et al. 2008).

The mesoscale air–sea coupling is pronounced in all of the western boundary current systems and in other regions where strong SST gradients exist. The thermodynamic similarity between SST gradient forcing and topographic forcing on the near-surface wind variability suggests a possible connection between surface air–sea coupling and free tropospheric variability, a similar influence to that of topography. Minobe et al. (2008) recently reported that the Gulf Stream affects the entire troposphere. It is therefore important that this type of air–sea coupling be accurately simulated with improved PBL vertical mixing parameterizations and high-resolution SST boundary conditions. The accuracy of mesoscale air–sea coupling in the NWP and climate models not only benefits the meteorological community, but also improves the NWP wind fields that are used to force ocean circulation. It should be mentioned that the mesoscale air–sea coupling obtained from the NCEP NWP model (not shown here) is similar to that from the ECMWF operational model. The conclusions presented here for the ECMWF model are thus also applicable to the NCEP NWP model. Presently, the NCEP model continues to use the Reynolds SST analyses as the ocean surface boundary condition. As a consequence, the surface wind speed fields in the NCEP model are even more deficient on short scales than in the ECMWF model.

Acknowledgments. We thank Michael Schlax and Craig Risien for their help preparing the QuikSCAT wind speed and AMSR SST fields analyzed in this study. This research was conducted with support from NASA Grant NAS5-32965 for funding of Ocean Vector Winds Science Team activities and Award NA03NES4400001 to Oregon State University's Cooperative Institute for Oceanographic Satellite Studies from the National Oceanic and Atmospheric Administration, U.S. Department of Commerce. The statements, findings, conclusions, and recommendations expressed here are those of the authors and do not necessarily reflect the views of the National Oceanic and Atmospheric Administration, the U.S. Department of Commerce, or the National Aeronautics and Space Administration.

REFERENCES

Bretherton, C. S., J. R. McCaa, and H. Grenier, 2004: A new parameterization for shallow cumulus convection and its application to marine subtropical cloud-topped boundary layers. Part I: Description and 1D results. *Mon. Wea. Rev.,* **132,** 864–882.

Brown, A. R., A. C. M. Beljaars, H. Hersbach, A. Hollingsworth, M. Miller, and D. Vasiljevic, 2005: Wind turning across the marine atmospheric boundary layer. *Quart. J. Roy. Meteor. Soc.,* **131,** 1233–1250.

——, ——, and ——, 2006: Errors in parameterizations of convective boundary-layer turbulent momentum mixing. *Quart. J. Roy. Meteor. Soc.,* **132,** 1859–1876.

——, R. J. Beare, J. M. Edwards, A. P. Lock, S. J. Keogh, S. F. Milton, and D. N. Walters, 2008: Upgrades to the boundary layer scheme in the Met Office NWP model. *Bound.-Layer Meteor.,* **128,** 117–132.

Businger, J. A., and W. J. Shaw, 1984: The response of the marine boundary layer to mesoscale variation in sea-surface temperature. *Dyn. Atmos. Oceans,* **8,** 267–281.

Cavaleri, L., L. Bertotti, M. Hortal, and M. Miller, 1997: Effect of reduced diffusion on surface wind and wave fields. *Mon. Wea. Rev.,* **125,** 3024–3029.

Chelton, D. B., 2005: The impact of SST specification on ECMWF surface wind stress fields in the eastern tropical Pacific. *J. Climate,* **18,** 530–550.

——, and F. J. Wentz, 2005: Global microwave satellite observations of sea surface temperature for numerical weather prediction and climate research. *Bull. Amer. Meteor. Soc.,* **86,** 1097–1115.

——, and Coauthors, 2001: Observations of coupling between surface wind stress and sea surface temperature in the eastern tropical Pacific. *J. Climate,* **14,** 1479–1498.

——, M. G. Schlax, M. H. Freilich, and R. F. Milliff, 2004: Satellite measurements reveal persistent small-scale features in ocean winds. *Science,* **303,** 978–983.

Durran, D. R., 2000: Comments on "The differentiation between grid spacing and resolution and their application to numerical modeling." *Bull. Amer. Meteor. Soc.,* **81,** 2478.

Friehe, C. A., and Coauthors, 1991: Air-sea fluxes and surface layer turbulence around a sea surface temperature front. *J. Geophys. Res.,* **96,** 8593–8609.

Galperin, B., L. H. Kantha, S. Hassid, and A. Rosati, 1988: A quasi-equilibrium turbulent energy model for geophysical flows. *J. Atmos. Sci.,* **45,** 55–62.

Giordani, H., S. Planton, B. Benech, and B.-H. Kwon, 1998: Atmospheric boundary layer response to sea surface temperatures during the SEMAPHORE experiment. *J. Geophys. Res.,* **103,** 25 047–25 060.

Grasso, L. D., 2000: The differentiation between grid spacing and resolution and their application to numerical modeling. *Bull. Amer. Meteor. Soc.,* **81,** 579–580.

Grenier, H., and C. S. Bretherton, 2001: A moist PBL parameterization for large-scale model and its application to subtropical cloud-topped marine boundary layers. *Mon. Wea. Rev.,* **129,** 357–377.

Haack, T., S. D. Burk, and R. M. Hodur, 2005: U.S. west coast surface heat fluxes, wind stress, and wind stress curl from a mesoscale model. *Mon. Wea. Rev.,* **133,** 3202–3216.

——, D. B. Chelton, J. Pullen, J. Doyle, and M. Schlax, 2008: Summertime influence of SST on surface wind stress off the U.S. West Coast from the U.S. Navy COAMPS model. *J. Phys. Oceanogr.,* **38,** 2414–2437.

Janjic, Z. I., 2002: Nonsingular implementation of the Mellor–Yamada level 2.5 scheme in the NCEP meso models. NCEP Office Note 437, 61 pp.

Lee-Thorp, A. M., M. Rouault, and J. R. E. Lutjeharms, 1999: Moisture uptake in the boundary layer above the Agulhas Current: A case study. *J. Geophys. Res.,* **104,** 1423–1430.

Maloney, E. D., and D. B. Chelton, 2006: An assessment of the sea surface temperature influence on surface wind stress in numerical weather prediction and climate models. *J. Climate,* **19,** 2743–2762.

Mellor, G., and T. Yamada, 1982: Development of a turbulent closure model for geophysical fluid problems. *Rev. Astrophys. Space Phys.,* **20,** 851–875.

Minobe, S., A. Kuwano-Yoshida, N. Komori, S.-P. Xie, and R. J. Small, 2008: Influence of the Gulf Stream on the troposphere. *Nature,* **452,** 206–209.

O'Neill, L. W., D. B. Chelton, and S. K. Esbensen, 2003: Observations of SST-induced perturbations of the wind stress field over the Southern Ocean on seasonal timescales. *J. Climate,* **16,** 2340–2354.

——, ——, ——, and F. J. Wentz, 2005: High-resolution satellite measurements of the atmospheric boundary layer response to SST variations along the Agulhas Return Current. *J. Climate,* **18,** 2706–2723.

——, ——, ——, and N. Thum, 2008: The effects of SST-induced horizontal surface wind speed and direction gradients on midlatitude vorticity and divergence fields: Observations and numerical simulation. *J. Climate,* submitted.

Park, K.-A., and P. Cornillon, 2002: Stability-induced modification of sea surface winds over Gulf Stream rings. *Geophys. Res. Lett.,* **29,** 2211, doi:10.1029/2001GL014236.

——, ——, and D. L. Codiga, 2006: Modification of surface winds near ocean fronts: Effects of Gulf Stream rings on scatterometer (QuikSCAT, NSCAT) wind observations. *J. Geophys. Res.,* **111,** C03021, doi:10.1029/2005JC003016.

Pielke, R. A., 1991: A recommended specific definition of "resolution." *Bull. Amer. Meteor. Soc.,* **72,** 1914.

Reynolds, R. W., T. M. Smith, C. Liu, D. B. Chelton, K. S. Casey, and M. G. Schlax, 2007: Daily high-resolution-blended analyses for sea surface temperature. *J. Climate,* **20,** 5474–5496.

Rouault, M., C. J. C. Reason, J. R. E. Lutjeharms, and A. C. M. Beljaars, 2003: Underestimation of latent and sensible heat fluxes above the Agulhas Current in NCEP and ECMWF analyses. *J. Climate,* **16,** 776–782.

Skamarock, W. C., 2004: Evaluating mesoscale NWP models using kinetic energy spectra. *Mon. Wea. Rev.,* **132,** 3019–3032.

——, J. B. Klemp, J. Dudhia, D. O. Gill, D. M. Barker, W. Wang, and J. G. Powers, 2005: A description of the advanced research WRF version 2. NCAR Tech. Note NCAR/TN468+STR, 88 pp.

Small, R. J., S.-P. Xie, and Y. Wang, 2003: Numerical simulation of atmospheric response to Pacific tropical instability waves. *J. Climate,* **16,** 3723–3741.

——, ——, ——, S. K. Esbensen, and D. Vickers, 2005: Numerical simulation of boundary layer structure and cross-equatorial flow in the eastern Pacific. *J. Atmos. Sci.,* **62,** 1812–1830.

——, and Coauthors, 2008: Air-sea interaction over ocean fronts and eddies. *Dyn. Atmos. Oceans,* **45,** 274–319.

Song, Q., T. Hara, P. Cornillon, and C. A. Friehe, 2004: A comparison between observations and MM5 simulations of the

marine atmospheric boundary layer across a temperature front. *J. Atmos. Oceanic Technol.,* **21,** 170–178.

——, P. Cornillon, and T. Hara, 2006: Surface wind response to oceanic fronts. *J. Geophys. Res.,* **111,** C12006, doi:10.1029/2006JC003680.

Spall, M. A., 2007: Midlatitude wind stress–sea surface temperature coupling in the vicinity of ocean fronts. *J. Climate,* **20,** 3785–3801.

Sweet, W., R. Fett, J. Kerling, and P. LaViolette, 1981: Air–sea interaction effects in the lower troposphere across the north wall of the Gulf Stream. *Mon. Wea. Rev.,* **109,** 1042–1052.

Tang, W., and W. T. Liu, 1996: Equivalent neutral wind. Jet Propulsion Laboratory Publication 96-17, 8 pp.

Walters, M. K., 2000: Comments on "The differentiation between grid spacing and resolution and their application to numerical modeling." *Bull. Amer. Meteor. Soc.,* **81,** 2475–2477.

Xie, S.-P., 2004: Satellite observations of cool ocean–atmosphere interaction. *Bull. Amer. Meteor. Soc.,* **85,** 195–208.